PROCEEDINGS OF SCIENCE

Hamiltonian limit of lattice QED in 2+1 dimensions

L. Funcke,[a,b] **C. F. Groß,**[c,*] **K. Jansen,**[d] **S. Kühn,**[d,e] **S. Romiti**[c,*] **and C. Urbach**[c]

[a] *Transdisciplinary Research Area "Building Blocks of Matter and Fundamental Interactions" (TRA Matter) and Helmholtz Institute for Radiation and Nuclear Physics (HISKP), University of Bonn, Nußallee 14-16, 53115 Bonn, Germany*

[b] *Center for Theoretical Physics, Co-Design Center for Quantum Advantage, and NSF AI Institute for Artificial Intelligence and Fundamental Interactions, Massachusetts Institute of Technology, 77 Massachusetts Avenue, Cambridge, MA 02139, USA*

[c] *HISKP and Bethe Center for Theoretical Physics, Rheinische Friedrich-Wilhelms-Universität Bonn, Nußallee 14-16, 53115 Bonn, Germany*

[d] *Deutsches Elektronen-Synchrotron DESY, Platanenallee 6, 15738 Zeuthen, Germany*

[e] *Computation-Based Science and Technology Research Center, The Cyprus Institute, 20 Kavafi Street, 2121 Nicosia, Cyprus*

E-mail: lfuncke@uni-bonn.de, christiane.gross@uni-bonn.de, karl.jansen@desy.de, stefan.kuehn@desy.de, simone.romiti@uni-bonn.de, urbach@hiskp.uni-bonn.de

The Hamiltonian limit of lattice gauge theories can be found by extrapolating the results of anisotropic lattice computations, i.e., computations using lattice actions with different temporal and spatial lattice spacings ($a_t \neq a_s$), to the limit of $a_t \to 0$. In this work, we present a study of this Hamiltonian limit for a Euclidean $U(1)$ gauge theory in 2+1 dimensions (QED3), regularized on a toroidal lattice. The limit is found using the renormalized anisotropy $\xi_R = a_t/a_s$, by sending $\xi_R \to 0$ while keeping the spatial lattice spacing constant. We compute ξ_R in 3 different ways: using both the "normal" and the "sideways" static quark potential, as well as the gradient flow evolution of gauge fields. The latter approach will be particularly relevant for future investigations of combining quantum computations with classical Monte Carlo computations, which requires the matching of lattice results obtained in the Hamiltonian and Lagrangian formalisms.

The 39th International Symposium on Lattice Field Theory, LATTICE2022
8-13 August 2022
Hörsaalzentrum Poppelsdorf, Bonn, Germany

*Speaker

PoS(LATTICE2022)292

1. Introduction

The idea of studying gauge theories on a space-time lattice dates back to 1974-75 [1, 2]. Since then, most numerical simulations have been performed in the Lagrangian formalism, using path integral Monte Carlo techniques at imaginary time [3]. However, in recent years, we have been witnessing a rapid development of Hamiltonian-based simulations using, e.g., tensor networks [4] or quantum computing [5]. In particular, the rapid development of quantum technology [6] may open a window for phenomenologically relevant Hamiltonian simulations on quantum computers in the future. Although there is still a long way to go from both the theoretical and technological perspective, first proof-of-concept simulations of lower-dimensional gauge theories have already been performed using quantum computers (see, e.g., Ref. [7] for a recent review).

In the continuum limit, the Lagrangian and Hamiltonian formalisms are equivalent [8, 9]. On the lattice, the Hamiltonian limit is obtained by sending the temporal lattice spacing to zero, $a_t \to 0$, using an *anisotropic* lattice action [10–12]. The anisotropy is introduced through an additional parameter in the lattice action, called the *bare anisotropy* ξ_0. For $\xi_0 \neq 1$, this parameter breaks the symmetry between the temporal and spatial contributions. The resulting *renormalized anisotropy* $\xi_R = a_t/a_s$, defined as the ratio between the temporal and spatial lattice spacings, also deviates from 1. The Hamitonian limit can be found by sending $\xi_R \to 0$, while keeping a_s fixed.

At finite lattice spacing, there is a non-trivial dependence between the bare parameters and the observables in the Lagrangian and Hamiltonian formalisms, and a matching is required. This can be done in two ways. First, at a given spatial lattice spacing a_s, one can match the bare parameters g_i to equally many observables O_i, either perturbatively or non-perturbatively. Second, one can perform a set of Lagrangian simulations at decreasing temporal lattice spacing a_t, extrapolating to the Hamiltonian limit ($a_t \to 0$) in parameter space.

In this work, we explore the latter approach for a $U(1)$ gauge theory in $2+1$ dimensions. In the literature, this theory is often referred to as QED 2+1 (see, e.g., Refs. [13–17]) or QED3 (see, e.g, Refs. [18–23]). We choose to study this theory due to the recent proposal of Ref. [24] to combine quantum computations of QED 2+1 with classical Monte Carlo computations, which requires a matching of the lattice results obtained in the Hamiltonian and Lagrangian formalisms. The generalisation of our study to higher dimensions and $SU(N)$ theories could be straight-forwardly done with simple theoretical modifications, but would of course be computationally challenging. We note that QED 2+1 is not only relevant for condensed matter systems [25], but also exhibits confinement [26] and dynamical mass generation [27]. These features make it a toy model for QCD and a benchmark model for the study of lattice gauge theories. Most crucially, due to its simple structure, QED 2+1 offers the possibility of near-future simulations in the Hamiltonian formalism using quantum hardware (see, e.g., Ref. [24, 28, 29]).

An important advantage of Hamiltonian simulations is the absence of specific numerical issues in Monte Carlo simulations, in particular the sign problem [30] and the problem of critical slowing down [12]. Therefore, in general, matching the two formalisms allows to span the whole parameter space and to improve the continuum limit by adding more points to the extrapolation.

The rest of the paper is organized as follows. In Sec. 2, we introduce the lattice action and some theoretical aspects of the Hamiltonian limit. Section 3 shows how to compute ξ_R using the static potential, and Sec. 4 the Hamiltonian limit for the plaquette expectation value. In Sec. 5, we discuss

the calculation of ξ_R using the gradient flow. In Sec. 6, we provide conclusions and an outlook.

2. Theoretical background

In this work, we study a Euclidean $U(1)$ gauge theory on a periodic (2+1)-dimensional lattice of size $\Lambda = L^2 \times T = (N_s a_s)^2 \times (N_t a_t)$, where N_t (N_s) is the number of lattice sites in the temporal (spatial) direction, separated by a lattice spacing a_t (a_s). We use the compact formulation [31, 32] of the lattice gauge theory, where the degrees of freedom are the link operators $U_\mu(x) = \exp(i a_\mu A_\mu(x))$ at each lattice point $x \in \Lambda$ with direction μ. The ultraviolet and infrared divergences in the photon propagator [33] are automatically regularised by the finite lattice spacing and volume.

The dynamics of the U(1) gauge theory is described by the standard Wilson action:

$$S_W = \frac{\beta}{\xi_0} \sum_{x,i} \mathrm{Re}\,(1 - P_{0i}(x)) + \beta \xi_0 \sum_{x,i>j} \mathrm{Re}\left(1 - P_{ij}(x)\right), \tag{1}$$

where $P_{\mu\nu}$ is the plaquette operator:

$$P_{\mu\nu} = U_\mu(x)\, U_\nu(x+\hat{\mu})\, U_\mu^\dagger(x+\hat{\nu})\, U_\nu^\dagger(x)\,. \tag{2}$$

In the action above, we took into account that $P_{\mu\nu} = 1$ for $\mu = \nu$ and that the trace operator for the $U(1)$ gauge theory is trivial. Moreover, we defined $\beta = 2/g^2$, where g is the gauge coupling. The parameter ξ_0 is the bare anisotropy, which induces an asymmetry between the temporal and spatial parts of the action, measured by the *renormalized anisotropy* $\xi_R = a_t/a_s$. We note that for $\xi_0 = 1$ the action is symmetric, which implies $\xi_R = 1$. However, for $\xi_0 = 0$ we *de facto* remove one dimension and hence simulate a different lattice theory. This implies that the Hamiltonian limit of $\xi_R \to 0$ does not coincide with the naive limit of $\xi_0 \to 0$. Thus, the renormalized anisotropy ξ_R depends on the coupling β. In Secs. 3 and 5, we describe how ξ_R can be determined using the quark static potential and the gradient flow evolution of gauge fields, respectively.

Instead of using the standard Wilson lattice action in Eq. (1) with the continuum limit $\sim F_{\mu\nu}F_{\mu\nu}$ [34], we could have also used a different lattice action with the same continuum limit but other linear combinations of links loops. Some lattice actions lead to smaller discretization effects [35, 36], thus reducing the difference between ξ_R and ξ_0 [10]. Here, however, we intentionally focus on the action in Eq. (1), because the corresponding Hamiltonian is currently more feasible to simulate.

The results for the observables presented in the following sections have been calculated using the library provided in Ref. [37], with which we also generated the gauge configuration samples. The statistical analysis was done with routines provided in Ref. [38].

3. Renormalized anisotropy from the static potential

At finite lattice spacing, the U(1) gauge theory in 2+1 dimensions is a confining theory [15, 39], with the potential energy $V(r)$ between two static quark charges, q and $\bar{q}$, given by [40–43]

$$V(r) = a + \sigma\, r + b \log(r)\,. \tag{3}$$

Here r is the distance separating q and $\bar{q}$, and σ is the *string tension*. On the lattice, $V(r)$ is found from the large-distance behaviour of the expectation value of Wilson loops [12],

$$\lim_{x_\mu \to \infty} \frac{W(x_\mu + a_\mu \hat{\mu}, r)}{W(x_\mu, r)} = \exp(-a_\mu V(r)) \,, \tag{4}$$

where μ is any direction on the space-time lattice. In the following, we use the conventions $x_\mu = (t, x, y)$ and $\hat{\mu} = (\hat{t}, \hat{x}, \hat{y})$. We consider planar Wilson loops, where r is the separation between the starting point and the end point of the first half of the loop along a plane perpendicular to the μ direction. Which plane we refer to becomes clear from the chosen r coordinate, e.g., the Wilson loop $W(t, x)$ refers to a rectangular loop in the $\hat{t} - \hat{x}$ plane with $r = x$.

The higher energy states in Eq. (4) contribute at finite x_μ, but become exponentially suppressed as x_μ increases. Therefore, the potential is found from a fit to a constant of the corresponding effective curve in the large-x_μ region,

$$a_\mu V^{\text{eff}}(x_\mu, r) = \log\left(\frac{W(x_\mu, r)}{W(x_\mu + a_\mu \hat{\mu}, r)}\right). \tag{5}$$

On the lattice, we can only compute quantities in lattice units, so the potential in Eq. (5) is measured in units of a_μ. On isotropic lattices, we get the same potential for any μ, but on anisotropic lattices, i.e., for $\xi_0 \neq 1$, there is a difference between the *spatial-spatial* and *temporal-spatial* loops, which encodes the renormalized anisotropy ξ_R.

In this study, we compute the *temporal* static quark potential with both the *normal* [10] and *sideways* [44] methods, which we will explain below, see Eqs. (7) and (9). We will later use two different approaches to determine the anisotropy ξ_R, see Eqs. (8) and (10), and will use the normal (sideways) *temporal* quark potential for the first (second) approach. The *spatial* static quark potential is always computed as

$$\lim_{x \to \infty} \frac{W(x+1, y)}{W(x, y)} = \exp(-a_s V(y[a_s])), \tag{6}$$

and is used for both ways of determining the anisotropy, i.e., for both Eqs. (8) and (10) below. We note that in Eq. (6), x and y are treated on the same footing and thus can be exchanged.

Normal potential. The normal temporal potential is calculated as

$$\lim_{t \to \infty} \frac{W(x, t+1)}{W(x, t)} = \exp(-a_t V(x[a_s])), \tag{7}$$

where a_t is the temporal lattice spacing. In Eqs. (6) and (7), the left-hand sides are equal for $\xi_0 = 1$ but they differ due to anisotropy effects. Thus, as shown in Fig. 1(a), we find the renormalized anisotropy ξ_R through a linear fit of $a_s V(x)$ against $a_t V(x)$,

$$(a_s V(x)) = \frac{1}{\tilde{\xi}_R} (a_t V(x)) + \tilde{C} \,, \tag{8}$$

where $\tilde{C}$ is a constant and $\tilde{\xi}_R$ is an estimator for the renormalized anisotropy ξ_R. Here, both $\tilde{\xi}_R$ and $\tilde{C}$ are treated as free parameters of the fit (see the left panel of Fig. 1), and $\tilde{C}$ is the usual arbitrary shift in the potential energy [45]. This method is adapted from the one proposed in Ref. [10].

Sideways potential. Analogously, the sideways temporal potential is determined from

$$\lim_{x\to\infty} \frac{W(x+1,t)}{W(x,t)} = \exp(-a_s V(t[a_t]))\,. \tag{9}$$

Following Ref. [44], the anisotropy is calculated by performing a piecewise linear interpolation of the temporal potential [see Eq. (9)]. We build the polygonal chain of the temporal potential curve $V(t[a_t])$ as a function of the temporal distance t/a_t. Then, we restrict ourselves to the points in the linear region, for which $V(r) \approx \sigma r$ [see Eq. (3)] by requiring $r/a_s \geq 2$. For each point of the spatial potential at distance y/a_s in this region, we find the temporal distance t/a_t that matches the temporal and spatial values of the potential on the polygonal chain from the condition:

$$V(y[a_s]/\tilde{\xi}_R) = V(t[a_t])\,. \tag{10}$$

The $\tilde{\xi}_R$ needed to fulfill this equation is taken as the estimator for the renormalized anisotropy ξ_R. The final result for $\tilde{\xi}_R$ is computed by averaging over all points (see the right panel of Fig. 1).

The two methods using Eqs. (8) and (10), respectively, are summarised and compared in Fig. 1, showing good agreement for the resulting anisotropies $\tilde{\xi}_R$. In the remaining part of this paper, we will omit the tilde for brevity and call the numerically determined anisotropies ξ_R.

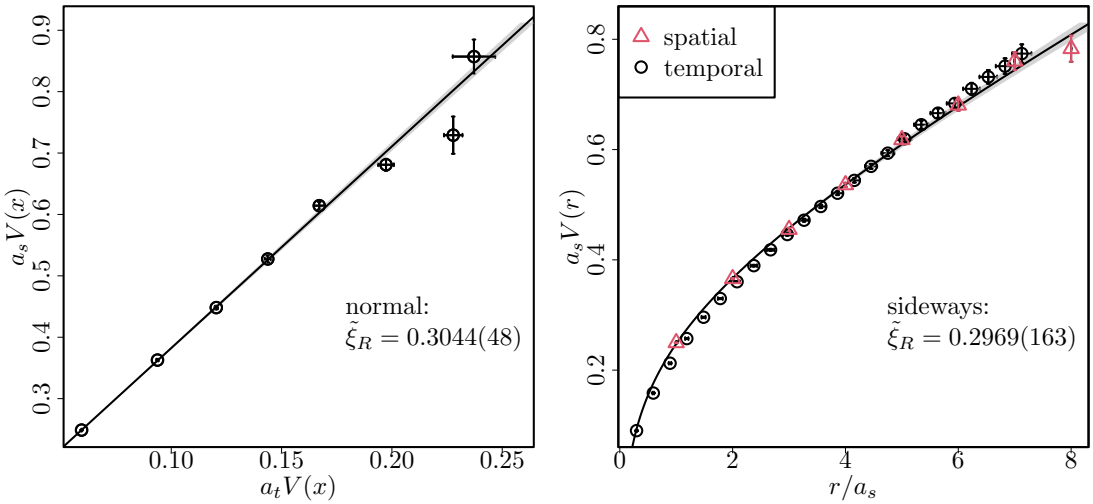

Figure 1: The normal and sideways potentials at $\beta = 1.7$, $L/a_s = 16$, and $\xi_0 = 1/3$. Left: the normal potentials are fit to Eq. (8). Right: the sideways potentials are fit to Eq. (3). The temporal sideways potential is rescaled with $\tilde{\xi}_R$, in order to be in units of a_s, with $\tilde{\xi}_R$ as determined from Eq. (10).

4. Hamiltonian limit of the plaquette expectation value

The naive Hamiltonian limit is reached by sending $\xi_0 \to 0$, while keeping β fixed (see, e.g., Ref. [43]). However, this is only approximately correct because β renormalizes as well, and the discretization effects grow significantly when approaching $\xi_0 \to 0$. Figure 2(a) shows the failure of this naive approach for the plaquette expectation value $\langle P \rangle$.

In order to take the correct Hamiltonian limit, the inverse coupling β needs to be adjusted, such that the spatial lattice spacing a_s stays constant. While this has been previously investigated on the

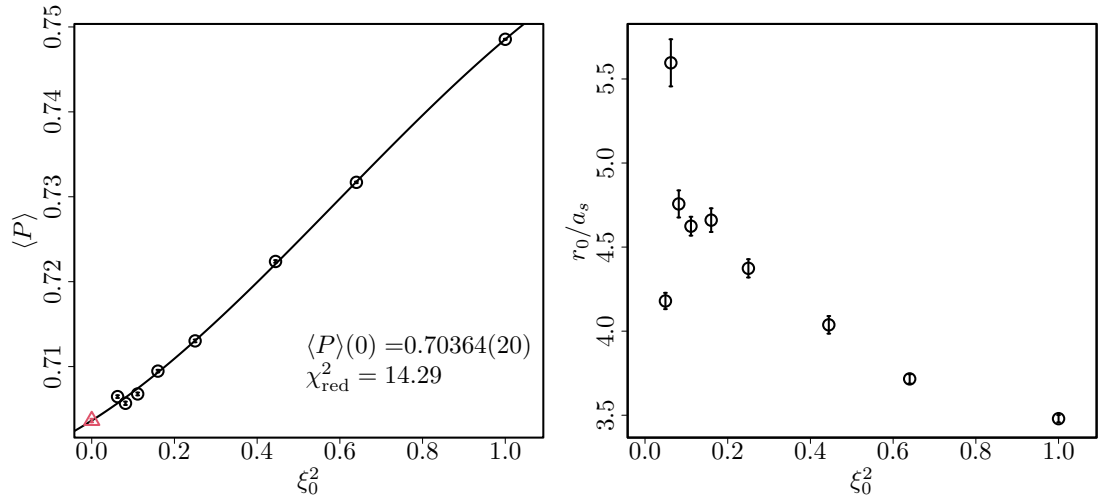

Figure 2: Left: naive Hamiltonian limit $\xi_0 \to 0$ of the plaquette expectation value with keeping β constant, using $\beta = 1.7$ and $L = 16$. The plaquette behaves non-monotonously at the smallest anisotropies, which results in a large χ^2_{red} of the cubic fit against ξ_0^2. Right: Sommer parameter in lattice units, r_0/a_s, is not constant as a function of ξ_0^2, explaining why the naive limit of $\xi_0 \to 0$ keeping β constant is not sufficient.

perturbative level [46, 47], in our work we focus on a general non-perturbative procedure, which is independent of the coupling strength.

What one should do is to compute the renormalized anisotropy ξ_R, using either the static potential (see Sec. 3) or the gradient flow (see Sec. 5), and send $\xi_R \to 0$ while keeping a_s fixed. We then first define the spatial lattice spacing a_s in terms of the Sommer parameter r_0 [48]. Analogously to QCD, we impose the condition [48]

$$-r^2 \frac{\mathrm{d}}{\mathrm{d}r} V(r)|_{r=r_0} = c_s = -1.65. \tag{11}$$

The value of c_s is arbitrary, but is usually chosen such that the point $V(r_0)$ lies in the region where $V(r)$ is approximately linear. The resulting value for r_0 should be in an intermediate region, because the small-r region is hard to probe due to the lattice regularisation, while the large-r region results in a low signal-to-noise ratio in the Wilson loop correlator of Eq. (5). In QCD, its value is fixed to $c_s = -1.65$ resulting in $r_0 = 0.5$ fm [48] using experimental inputs; however, we note that this value worked out well also for our data.

The dimensionless constant c_s implicitly defines r_0. Thus, it is sufficient to keep $r_0/a_s = \bar{r}_0$ fixed throughout the extrapolation of $\xi_R \to 0$. For the extrapolation, we select a range of values for the bare anisotropy ξ_0 and, for each value of ξ_0, perform simulations at different values of β. Starting from one of these ensembles, we keep $\bar{r}_0$ fixed by interpolating the ensembles with the same ξ_0 in the different values of β (see Fig. 3). To be more precise, we start at $\beta = 1.7$ and $\xi_0 = 1$, compute $\bar{r}_0$, and this value for $\bar{r}_0$ we keep fixed (given by the horizontal line in Fig. 3). We then decrease ξ_0, keeping the physical volume approximately fixed. Thus, we increase the number T/a_t of temporal lattice points and keep fixed the number of spatial lattice points, $L/a_s = 16$, such that $\xi_0 \equiv L/T$. The physical volume does not change much ($\xi_0 \approx \xi_R$, see Fig. 1), leading to similar finite-volume effects. For a given value of ξ_0, we simulate at different bare couplings β and fit

$\bar{r}_0$ linearly against β, which gives us the value of the renormalized coupling β_R, defined through $\bar{r}_0(\beta_\mathrm{R}, \xi_0) = \bar{r}_0(\beta = 1.7, \xi_0 = 1)$ (see the intersecting lines in Fig. 3). Note that we call the coupling β_R "renormalized" in the sense that is renormalized in a_t but not in a_s. Finally, we interpolate the renormalized anisotropy ξ_R and the plaquette expectation value $\langle P \rangle$ linearly to the values of β determined from $\bar{r}_0$.

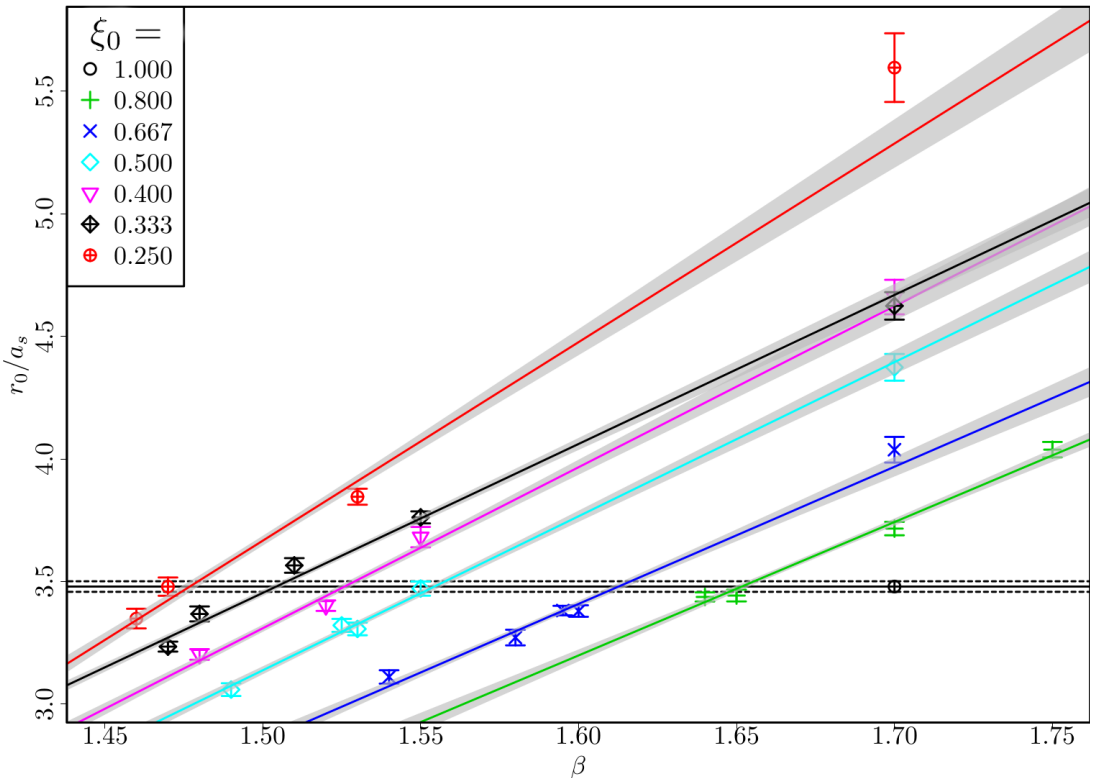

Figure 3: Numerical determination of the coupling β such that $\bar{r}_0$ stays constant (black horizontal line). Each marker (see legend) corresponds to a different value of ξ_0, and the colored lines are the best-fit interpolations at fixed ξ_0. The error bands are shown in faint grey. The intersections of the lines with the horizontal one (given by $\bar{r}_0 = \text{const.}$ for $\beta = 1.7$ and $\xi_0 = 1$) determine the values of β for which $\bar{r}_0 = \text{const.}$.

The left panel of Fig. 4 demonstrates how much the renormalized coupling β_R deviates from the bare coupling $\beta(\xi_0 = 1)$, i.e., how much the coupling needs to change in order to keep the spatial lattice spacing a_s constant. In the right panel, we show the resulting correct Hamiltonian limit of $\langle P \rangle$, which uses the renormalized β_R that changes with ξ_R, instead of keeping β fixed as in the naive Hamiltonian limit (see Fig. 2). For our initial parameters of $\beta = 1.7$ and $\xi_0 = 1$, the Hamiltonian limit of the plaquette expectation value is $\langle P \rangle\ (a_t = 0) = 0.6381(12)$, as determined with the normal potentials with $\chi^2_\mathrm{red} = 0.27$, or similarly $\langle P \rangle\ (a_t = 0) = 0.6365(14)$, as determined with the sideways potentials with $\chi^2_\mathrm{red} = 0.34$.

5. Renormalized anisotropy from the gradient flow

The renormalized anisotropy ξ_R can be determined using either the static potential (see Sec. 3) or the gradient flow evolution of gauge fields, as described in the current section. Using the static

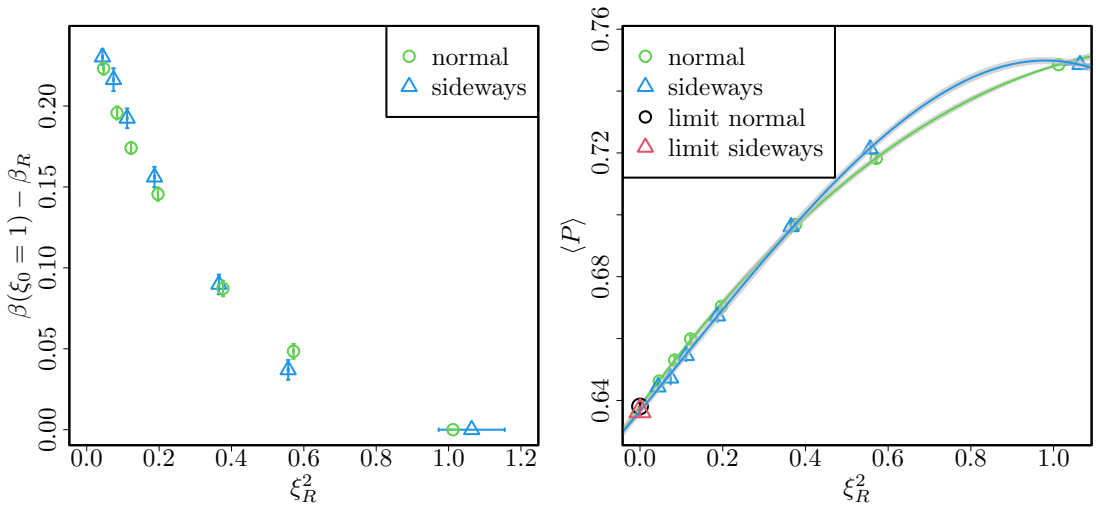

Figure 4: Left: deviation of the renormalized coupling β_R from the bare coupling $\beta(\xi_0 = 1)$, corresponding to the change in β required to keep a_s constant. Right: correct Hamiltonian limit of $\langle P \rangle$ using β_R instead of keeping β fixed. The extrapolation of $\langle P \rangle$ to $\xi_R \to 0$ is done with a simple cubic ansatz in ξ_R^2.

potential to find ξ_R has some drawbacks due to the extraction of the signal $V(r)$ from the Wilson loop correlator. The temporal extent of the lattice must be large enough, in order to find a plateau for $V(r)$ before the correlator signal degrades [49]. Besides this, $a_s V(r)$ increases with decreasing β [2]; thus, in the small-β region, the leading signal $\exp\{-tV(r)\}$ sooner ends below the statistical noise. It is therefore clear that another approach is needed to cover the full parameter space.

Analogously to QCD [50], we propose to use the Wilson gradient flow. First, we evolve in the flow time τ the gauge links $U_\mu(x,\tau)$ according to the flow equation [51, 52]

$$\frac{d}{d\tau} U_\mu(x,\tau) = -\frac{1}{\beta} \left[\nabla_\mu(x) S_W(U)\right] U_\mu(x,\tau)\,, \tag{12}$$

where $\nabla_\mu(x)$ is the covariant group derivative and S_W is the Wilson action defined in Eq. (1). Then, we find the flowed "gauge energies" as

$$E(\tau) = 2 \sum_x \sum_{\mu>\nu} \mathrm{Re\,Tr}\left[1 - P_{\mu\nu}(x,\tau)\right]\,. \tag{13}$$

At any flow time $\tau > 0$, both perturbation theory and numerical Lattice QCD results unveil that these quantities are already renormalized [51]. The electric (magnetic) energy E_{ts} (E_{ss}) can be obtained by summing over the temporal (spatial)-spatial plaquettes. Expanding the link operator $U_\mu(x,\tau) = \exp(i a_\mu A_\mu(x))$ to $O(a_s^4)$, we find:

$$E_{ts} \sim a_t^2 a_s^2 \sum_x \sum_i F_{0i}^2(x,\tau) = a_t^2 a_s^2 V(d-1)\tilde{E}_{ts}\,, \tag{14}$$

$$E_{ss} \sim a_s^4 \sum_x \sum_{i\neq j} F_{ij}^2(x,\tau) = a_s^4 V \frac{(d-1)(d-2)}{2} \tilde{E}_{ss}\,, \tag{15}$$

where V is the lattice volume, d is the number of dimensions, and $\tilde{E}_{ts}$ and $\tilde{E}_{ss}$ are the Euclidean average energy densities per space-time direction. In the continuum limit, there is no distinction

among directions, and each pair $\mu\nu$ gives the same contribution in physical units. In that limit, we have $\tilde{E}_{ts} = \tilde{E}_{ss}$; thus, ξ_R can be estimated (up to discretization effects) from the ratio

$$\zeta(\tau) = \sqrt{\frac{d-2}{2}\frac{E_{ts}(\tau)}{E_{ss}(\tau)}} \tag{16}$$

at a reference flow time τ_0, given by $\xi_R = \zeta(\tau_0)$. An advantage of this approach is that a few hundred representative configurations already give a small uncertainty. The reason is that the gradient flow smooths the fields, suppressing the discretization effects in the flowed plaquette [51].

As for r_0, the choice of τ_0 is arbitrary, and any positive value would lead to a renormalized quantity. From perturbation theory, we know that the flowed total energy (in physical units) goes as $E(\tau) \sim g^2\tau^{-d/2}$ [51]. We also recall that, in natural units, $[g] = [\text{eV}]^{(4-d)/2}$ [34] and $[\tau] = [\text{eV}]^{-2}$ from the equations of motion (12); therefore, we can use the simple condition

$$\tau^2 E(\tau)|_{\tau=\tau_0} = c\,, \tag{17}$$

where c is a dimensionless constant. This procedure is illustrated in Fig. 5. To our knowledge,

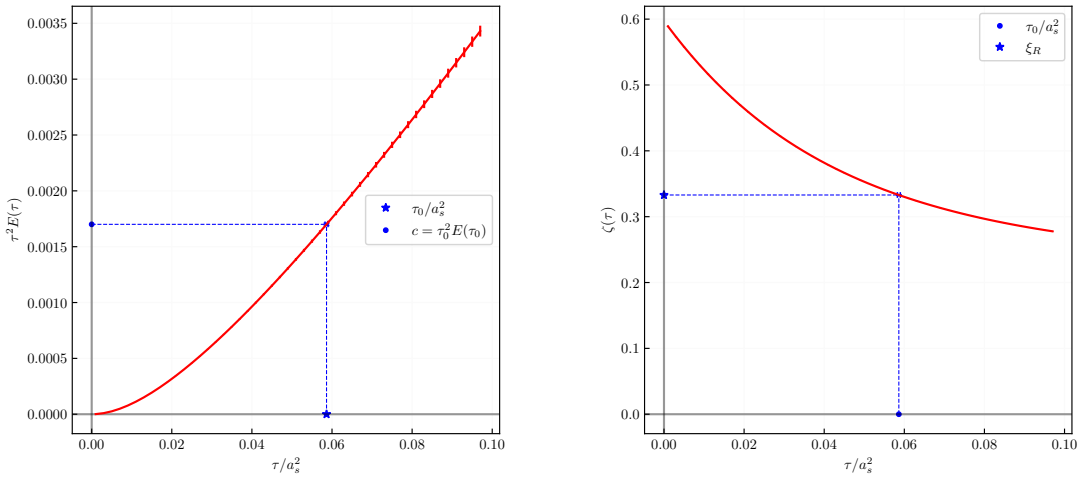

Figure 5: Left: fixing the reference flow time τ_0 from Eq. (17) (red curve), for the ensemble with $L = 16$, $\beta = 1.55$, and $\xi_0 = 0.4$. Right: determination of ξ_R using τ_0 from Eq. (16) (red curve), for the same ensemble. Note that both plots contain error bars, which are hard to visualize due to the small uncertainty of the flowed observables (see text).

the value of c for an Abelian $U(1)$ gauge theory in $2+1$ dimensions has not been determined yet, though we mention that in $3+1$ dimensions this was investigated for $SU(N_c)$ theories as a function of N_c [53]. We determine the value of c such that our results for ξ_R agree with the results for ξ_R obtained from the sideways static potential within 1σ, finding $c = 1.628(91) \cdot 10^{-3}$. This result has to be taken with a grain of salt, since it includes discretization effects also due to our prescription for r_0. The uncertainty gives the interval inside which the can vary c without spoiling the compatibility. In Fig. 6, we compare the values found with the two different approaches, using $c = 1.628 \cdot 10^{-3}$.

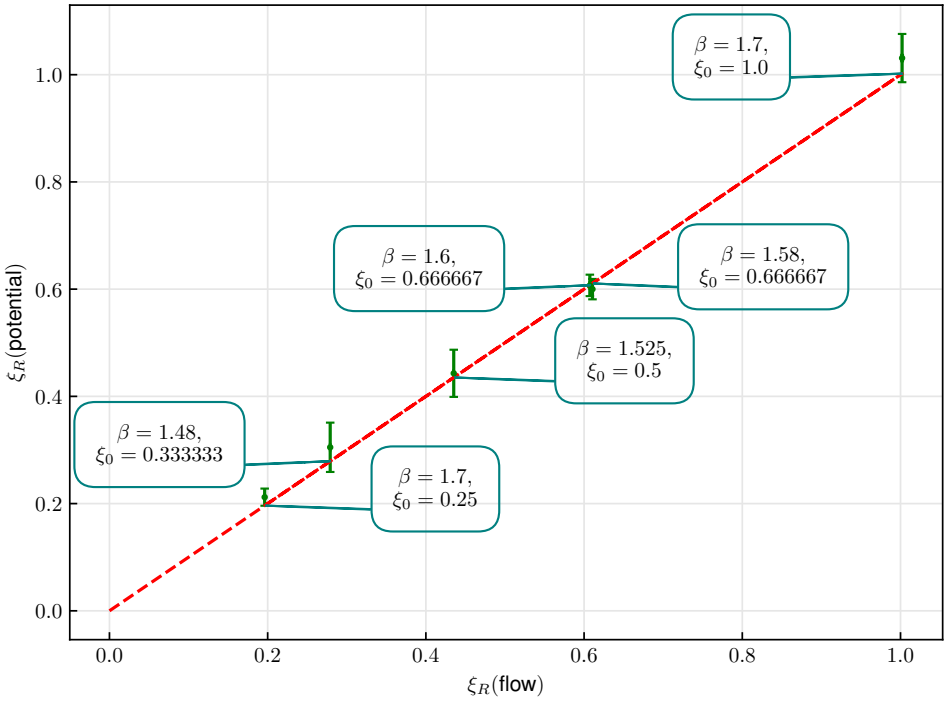

Figure 6: Renormalized anisotropy ξ_R determined with the static sideways potential, compared to ξ_R determined with the Wilson gradient flow using $c = 1.628 \cdot 10^{-3}$. Each point corresponds to an ensemble, labelled with its value of β and ξ_0. The red line, for which $y = x$, highlights how the choice of a single value for c yields a 1σ compatibility for all the ensembles. Note that the horizontal error bars are hardly visible due to the small uncertainty of ξ_R determined with the gradient flow (see text).

6. Conclusions and outlook

In this work, we have studied the Hamiltonian limit of Lattice QED in 2+1 dimensions. We have reviewed the issues related to taking this limit, showing an explicit numerical evidence that the naive limit of taking the temporal lattice spacing to zero, $a_t \to 0$, leads to the wrong result.

In particular, we have determined the Hamiltonian limit of the plaquette expectation value $\langle P \rangle$, along the parameter space trajectory passing through the point $\beta = 1.7$ and $\xi = 1$. For this, we have provided a non-perturbative prescription to keep the spatial lattice spacing a_s fixed, while sending the temporal lattice spacing to zero, $a_t \to 0$. This is done through the renormalized anisotropy $\xi_R = a_t/a_s$, moving along the curve $r_0/a_s = \text{const.}$.

We have discussed how to calculate ξ_R using the static quark potential $V(r)$, either the normal or sideways potential. This approach needs a good signal-to-noise ratio and a low excited-states contamination in the Wilson loop correlators, requiring large enough values of β and large enough volumes of the lattice. Following this observation, we investigated an alternative approach to determine ξ_R using the gradient flow, finding agreement with the first approach for large β. In the future, we aim to use this second approach in order to find ξ_R for small values of β. This will be particularly relevant for combining quantum computations with classical Monte Carlo computations (as proposed, e.g. in Ref. [24]), which requires the matching of lattice results obtained in the

Hamiltonian and Lagrangian formalisms.

Acknowledgements

This work is supported by the Deutsche Forschungsgemeinschaft (DFG, German Research Foundation) and the NSFC through the funds provided to the Sino-German Collaborative Research Center CRC 110 "Symmetries and the Emergence of Structure in QCD" (DFG Project-ID 196253076 - TRR 110, NSFC Grant No. 12070131001).

L.F. is partially supported by the U.S. Department of Energy, Office of Science, National Quantum Information Science Research Centers, Co-design Center for Quantum Advantage (C^2QA) under contract number DE-SC0012704, by the DOE QuantiSED Consortium under subcontract number 675352, by the National Science Foundation under Cooperative Agreement PHY-2019786 (The NSF AI Institute for Artificial Intelligence and Fundamental Interactions, http://iaifi.org/), and by the U.S. Department of Energy, Office of Science, Office of Nuclear Physics under grant contract numbers DE-SC0011090 and DE-SC0021006. S.K. acknowledges financial support from the Cyprus Research and Innovation Foundation under projects "Future-proofing Scientific Applications for the Supercomputers of Tomorrow (FAST)", contract no. COMPLEMENTARY/0916/0048, and "Quantum Computing for Lattice Gauge Theories (QC4LGT)", contract no. EXCELLENCE/0421/0019.

References

[1] K.G. Wilson, *Confinement of quarks*, *Phys. Rev. D* **10** (1974) 2445.

[2] J. Kogut and L. Susskind, *Hamiltonian formulation of Wilson's lattice gauge theories*, *Phys. Rev. D* **11** (1975) 395.

[3] Y. Aoki, T. Blum, G. Colangelo, S. Collins, M.D. Morte, P. Dimopoulos et al., *FLAG review 2021*, *Eur. Phys. J. C* **82** (2022) 1.

[4] M.C. Bañuls, K. Cichy, J.I. Cirac, K. Jansen and S. Kühn, *Tensor Networks and their use for Lattice Gauge Theories*, *PoS(Lattice 2018)* **0022** (2018) .

[5] M.C. Bañuls and et.al., *Simulating lattice gauge theories within quantum technologies*, *Eur. Phys. J. D* **74** (2020) .

[6] S.S. Gill, A. Kumar, H. Singh, M. Singh, K. Kaur, M. Usman et al., *Quantum computing: A taxonomy, systematic review and future directions*, *Softw. - Pract. Exp.* **52** (2022) 66.

[7] N. Klco, A. Roggero and M.J. Savage, *Standard Model Physics and the Digital Quantum Revolution: Thoughts about the Interface*, *Rep. Prog. Phys.* **85** (2022) 064301.

[8] R.P. Feynman, *Space-Time Approach to Non-Relativistic Quantum Mechanics*, *Rev. Mod. Phys.* **20** (1948) 367.

[9] P.A. Dirac, *The Lagrangian in quantum mechanics*, in *Feynman's Thesis—A New Approach To Quantum Theory*, pp. 111–119, World Scientific (2005), 10.1142/9789812567635_0003.

[10] M. Loan and C. Hamer, *Hamiltonian study of improved $U(1)$ lattice gauge theory in three dimensions*, *Phys. Rev. D* **70** (2004) .

[11] T.A. Degrand and C. DeTar, *Lattice Methods for Quantum Chromodynamics*, World Scientific (2006), 10.1142/6065.

[12] C. Gattringer and C. Lang, *Quantum Chromodynamics on the Lattice - an Introductory Presentation*, vol. 788, Springer Science & Business Media (2009), 10.1007/978-3-642-01850-3.

[13] A. Golub, S. Villalba-Chávez and C. Müller, *Strong-field Breit-Wheeler pair production in* QED_{2+1}, *Phys. Rev. D* **103** (2021) 096002.

[14] Zeitlin, Vadim, *Induced Magnetic Field in a Finite Fermion Density Maxwell QED* $2+1$, *Mod. Phys. Lett. A* **12** (1997) 877.

[15] Suzuki, Tsuneo and Shimada, Kayo, *Confinement Criteria and Compact (QED)* $2+1$, *Prog. Theor. Phys.* **69** (1983) 1537.

[16] A. Agarwal, *Antiparticles as Particles: QED* $2+1$ *and Composite Fermions at* $\nu = 1/2$, *Phys. Rev. Lett.* **123** (2019) 211601.

[17] M. Loan, M. Brunner, C. Sloggett and C. Hamer, *Path integral Monte Carlo approach to the* $U(1)$ *lattice gauge theory in* $2+1$ *dimensions*, *Phys. Rev. D* **68** (2003) 034504.

[18] S. Coleman and B. Hill, *No more corrections to the topological mass term in QED3*, *Phys. Lett. B* **159** (1985) 184.

[19] S.M. Chester and S.S. Pufu, *Towards bootstrapping QED3*, *J. High Energy Phys.* **2016** (2016) 1.

[20] M.R. Pennington and D. Walsh, *Masses from nothing. A non-perturbative study of QED3*, *Phys. Lett. B* **253** (1991) 246.

[21] N. Dorey and N.E. Mavromatos, *QED3 and two-dimensional superconductivity without parity violation*, *Nucl. Phys. B* **386** (1992) 614.

[22] S. Hands, J. Kogut and C. Strouthos, *Non-compact QED3 with* $N_f \geq 2$, *Nucl. Phys. B* **645** (2002) 321.

[23] D. Curtis, M.R. Pennington and D. Walsh, *Dynamical mass generation in QED3 and the 1/N expansion*, *Phys. Lett. B* **295** (1992) 313.

[24] G. Clemente, A. Crippa and K. Jansen, *Strategies for the Determination of the Running Coupling of* $(2+1)$*-dimensional QED with Quantum Computing*, *arXiv preprint arXiv:2206.12454* (2022) .

[25] P. Kosiński, P. Maślanka, J. Sławińska and I. Zasada, *QED_{2+1} in graphene: symmetries of Dirac equation in* $2+1$ *dimensions*, *Prog. Theor. Phys.* **128** (2012) 727.

[26] A. Athenodorou and M. Teper, *On the spectrum and string tension of $U(1)$ lattice gauge theory in $2+1$ dimensions*, *J. High Energy Phys.* **2019** (2019) 1.

[27] T.W. Appelquist, M. Bowick, D. Karabali and L.C.R. Wijewardhana, *Spontaneous chiral-symmetry breaking in three-dimensional QED*, *Phys. Rev. D* **33** (1986) 3704.

[28] J.F. Haase, L. Dellantonio, A. Celi, D. Paulson, A. Kan, K. Jansen et al., *A resource efficient approach for quantum and classical simulations of gauge theories in particle physics*, *Quantum* **5** (2021) 393 [2006.14160].

[29] D. Paulson et al., *Towards simulating 2D effects in lattice gauge theories on a quantum computer*, *PRX Quantum* **2** (2021) 030334 [2008.09252].

[30] C. Gattringer and K. Langfeld, *Approaches to the sign problem in lattice field theory*, *Int. J. Mod. Phys. A* **31** (2016) 1643007.

[31] S. Romiti, "The neutron proton mass difference in Lattice QCD+QED." Master's thesis, Roma Tre University, 2022.

[32] M. Panero, *A numerical study of confinement in compact QED*, *J. High Energy Phys.* **2005** (2005) 066.

[33] Z. Davoudi, J. Harrison, A. Jüttner, A. Portelli and M.J. Savage, *Theoretical aspects of quantum electrodynamics in a finite volume with periodic boundary conditions*, *Phys. Rev. D* **99** (2019) 034510.

[34] M.E. Peskin, *An Introduction To Quantum Field Theory*, CRC press (2018), 10.1201/9780429503559.

[35] K. Symanzik, *Continuum limit and improved action in lattice theories: (I). Principles and ϕ^4 theory*, *Nucl. Phys. B* **226** (1983) 187.

[36] Alford, M and Dimm, W and Lepage, GP and Hockney, G and Mackenzie, PB, *Lattice QCD on small computers*, *Phys. Lett. B* **361** (1995) 87.

[37] C.F. Groß, S. Romiti and C. Urbach, "su2 - Lattice simulations of $U(1)$ and $SU(2)$ in $d = 2, 3, 4$ dimensions." https://github.com/urbach/su2.

[38] C. Urbach and et al., "Hadron - An R implementation of fitting routines used in lattice QCD." https://github.com/HISKP-LQCD/hadron.

[39] J.B. Kogut, *An introduction to lattice gauge theory and spin systems*, *Rev. Mod. Phys.* **51** (1979) 659.

[40] A. Polyakov, *Thermal properties of gauge fields and quark liberation*, *Phys. Lett. B* **72** (1978) 477.

[41] M. Göpfert and G. Mack, *Proof of confinement of static quarks in 3-dimensional $U(1)$ lattice gauge theory for all values of the coupling constant*, *Commun. Math. Phys.* **82** (1982) 545.

[42] C. Borgs and E. Seiler, *Lattice Yang-Mills theory at nonzero temperature and the confinement problem*, *Commun. Math. Phys.* **91** (1983) 329.

[43] M. Loan, M. Brunner, C. Sloggett and C. Hamer, *Path integral Monte Carlo approach to the $U(1)$ lattice gauge theory in $2+1$ dimensions*, *Phys. Rev. D* **68** (2003) 034504.

[44] Alford, M. and Drummond, I. T. and Horgan, R. R. and Shanahan, H. and Peardon, M., *Measuring the aspect ratio renormalization of anisotropic-lattice gluons*, *Phys. Rev. D* **63** (2001) .

[45] D.J. Griffiths, *Introduction to electrodynamics*, American Association of Physics Teachers (2005), 10.1017/9781108333511.

[46] Carena, Marcela et al., *Gauge Theory Couplings on Anisotropic Lattices*, *arXiv preprint arXiv:2208.10417* (2022) .

[47] T.M.R. Byrnes, M. Loan, C.J. Hamer, F.D.R. Bonnet, D.B. Leinweber, A.G. Williams et al., *Hamiltonian limit of $(3+1)$-dimensional $SU(3)$ lattice gauge theory on anisotropic lattices*, *Phys. Rev. D* **69** (2004) .

[48] R. Sommer, *A new way to set the energy scale in lattice gauge theories and its application to the static force and α_s in $SU(2)$ Yang-Mills theory*, *Nucl. Phys. B* **411** (1994) .

[49] Lepage, G. Peter, *The Analysis of Algorithms for Lattice Field Theory*, in *Theoretical Advanced Study Institute in Elementary Particle Physics*, 6, 1989, https://inspirehep.net/literature/287173.

[50] S. Borsányi, S. Durr, Z. Fodor, S.D. Katz, S. Krieg, T. Kurth et al., *Anisotropy tuning with the Wilson flow*, *arXiv preprint arXiv:1205.0781* (2012) .

[51] M. Lüscher, *Properties and uses of the Wilson flow in lattice QCD*, *J. High Energy Phys.* **08** (2010) 071 [1006.4518].

[52] L. Mazur, "Applications of the Gradient flow method in lattice QCD." Master's thesis, Bielefeld University, 2017.

[53] T. DeGrand, *Simple chromatic properties of gradient flow*, *Phys. Rev. D* **95** (2017) 114512.